JACC: BASIC TO TRANSLATIONAL SCIENCE VOL. 8, NO. 10, 2023

LEADING EDGE TRANSLATIONAL RESEARCH

Targeting N-Myristoylation Through NMT2 Prevents Cardiac Hypertrophy and Heart Failure

Yusuke Tomita, MD,[a] Fumiya Anzai, MD, PhD,[a] Tomofumi Misaka, MD, PhD,[a,b] Ryo Ogawara, MD,[a] Shohei Ichimura, MD,[a] Kento Wada, MD, PhD,[a] Yusuke Kimishima, MD, PhD,[a] Tetsuro Yokokawa, MD, PhD,[a] Takafumi Ishida, MD, PhD,[a] Yasuchika Takeishi, MD, PhD[a]

VISUAL ABSTRACT

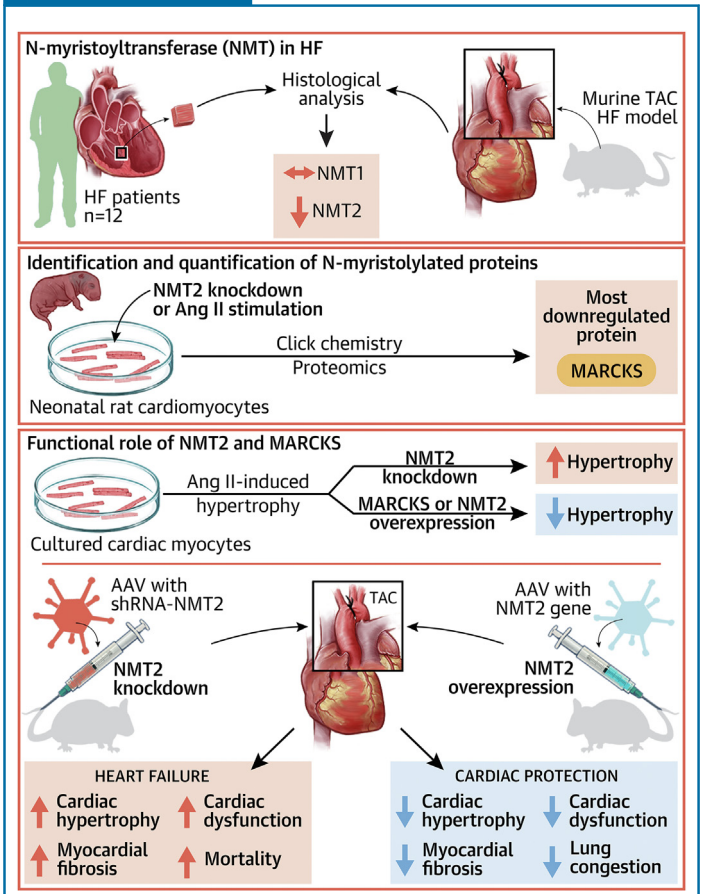

Tomita Y, et al. J Am Coll Cardiol Basic Trans Science. 2023;8(10):1263–1282.

HIGHLIGHTS

- **An innovative click chemistry–based quantitative proteomics demonstrates distinct global profiling of substrate proteins of N-myristoylation in cardiac myocytes at the endogenous level.**
- **NMT2 knockdown is maladaptive in a mouse model of pathological cardiac hypertrophy and failure.**
- **MARCKS was identified as a crucial substrate of N-myristoylation regulated by NMT2 and was found to prevent angiotensin II–induced cardiac pathological hypertrophy through the inhibition of activation of CaMKII and HDAC4 and histone acetylation.**
- **Up-regulation of N-myristoylation through AAV9-mediated transfer of the NMT2 gene to the heart attenuated pressure overload–induced cardiac remodeling and heart failure.**

From the [a]Department of Cardiovascular Medicine, Fukushima Medical University, Fukushima, Japan; and the [b]Department of Community Cardiovascular Medicine, Fukushima Medical University, Fukushima, Japan.
The authors attest they are in compliance with human studies committees and animal welfare regulations of the authors' institutions and Food and Drug Administration guidelines, including patient consent where appropriate. For more information, visit the Author Center.

Manuscript received May 1, 2023; revised manuscript received June 20, 2023, accepted June 20, 2023.

ISSN 2452-302X https://doi.org/10.1016/j.jacbts.2023.06.006

ABBREVIATIONS AND ACRONYMS

AAV9 = adeno-associated virus 9

Ang II = angiotensin II

CaMKII = Ca^{2+}/calmodulin-dependent protein kinase II

HDAC4 = histone deacetylase 4

IVSd = end-diastolic interventricular septum wall thickness

LC-MS/MS = liquid chromatography–tandem mass spectrometry

LVEF = left ventricular ejection fraction

mRNA = messenger RNA

MS = mass spectrometry

NMT = N-myristoyltransferase

NMT1 = N-myristoyltransferase 1

NMT2 = N-myristoyltransferase 2

NRCM = neonatal rat cardiomyocyte

PIP_2 = phosphatidylinositol 4,5-bisphosphate

PTM = post-translational modification

shRNA = short hairpin RNA

TAC = transverse aortic constriction

SUMMARY

Protein diversity can increase via N-myristoylation, adding myristic acid to an N-terminal glycine residue. In a murine model of pressure overload, knockdown of cardiac N-myristoyltransferase 2 (NMT2) by adeno-associated virus 9 exacerbated cardiac dysfunction, remodeling, and failure. Click chemistry-based quantitative chemical proteomics identified substrate proteins of N-myristoylation in cardiac myocytes. N-myristoylation of MARCKS regulated angiotensin II–induced cardiac pathological hypertrophy by preventing activations of Ca^{2+}/calmodulin-dependent protein kinase II and histone deacetylase 4 and histone acetylation. Gene transfer of NMT2 to the heart reduced cardiac dysfunction and failure, suggesting targeting N-myristoylation through NMT2 could be a potential therapeutic approach for preventing cardiac remodeling and heart failure.
(J Am Coll Cardiol Basic Trans Science 2023;8:1263–1282)

Heart failure involves structural changes in the heart such as hypertrophy, fibrosis, and dilatation, referred to as cardiac remodeling.[1] At the cellular level, cardiomyocytes undergo pathological hypertrophy characterized by increased cardiac muscle cell size, segregation of sarcomere structures, and enhanced protein synthesis by mechanical and neurohumoral stimuli, which drives the transitions to heart failure.[2] Post-translational modifications (PTMs) of proteins serve as a mechanism for increasing proteomic diversity that regulates the structure, localization, and interaction in cardiomyocytes,[3] which are essential for cardiovascular physiology and disease progression. Additionally, mutations of the post-translational target sites are directly involved in phenotype variation and types of cardiac diseases.[4] Prioritizing the regulators of PTMs in the cells is a promising therapeutic target to prevent or reverse cardiac remodeling as cardiomyocytes are terminally differentiated. Although global profiling of phosphorylation in the heart in response to β-agonists and in dilated cardiomyopathy has been reported,[5,6] direct comprehensive identification of protein substrates of living cells and pathological states is still challenging.

N-myristoylation is a key form of PTMs of proteins that entail the attachment of myristic acid to the N-terminal glycine residue.[7] N-myristoylation is catalyzed by N-myristoyltransferase (NMT) of N-myristoyltransferase 1 (NMT1) and N-myristoyltransferase 2 (NMT2) after the initiator methionine is eliminated by methionine aminopeptidase.[8] N-myristoylation plays a role in numerous physiological processes, including intracellular signaling, protein stability, and protein quality control.[9,10] In this regard, modifications of N-myristoylation are targeted in infectious diseases such as malaria,[11] sleeping sicknesses,[12] and neoplasms such as B-cell lymphomas.[13] It has been recently reported that N-myristoylation has a novel feature that mediates protein quality control as a glycine-specific N-end rule pathway to stabilize proteins.[14] Yet, the proteome of distinct N-myristoylation has not been investigated in cardiomyocytes, and it remains unclear if N-myristoylation in the heart is functionally relevant or how it is precisely regulated.

In this study, we aimed to clarify the pathological role and regulation of N-myristoylation in the heart and to determine proteome profiling of distinct N-myristoylation in cardiac myocytes. We applied quantitative chemical proteomics with a click chemistry-based approach for this purpose and demonstrate that targeting N-myristoylation through NMT2 is a novel potential therapeutic strategy for cardiac hypertrophy and heart failure.

METHODS

A detailed description of the methods is provided in the Supplemental Methods.

ANIMAL MODEL OF PRESSURE OVERLOAD BY TRANSVERSE AORTIC CONSTRICTION. Male mice with a C57BL/6 J background at 7 weeks old were subjected to transverse aortic constriction (TAC) or sham surgeries as previously reported.[15,16] A transsternal thoracotomy was performed after deep anesthesia was confirmed, and the aorta was constricted at the arch between the brachiocephalic artery and left common carotid artery by tying a 7.0 suture with a 27- or 28-gauge blunt needle as indicated.

PATIENT SUBJECTS. We enrolled patients with symptomatic stage C/D heart failure (n = 12) and age-matched and sex-matched non-heart failure

participants (n = 6), all of whom underwent endomyocardial biopsy at Fukushima Medical University Hospital between January 2016 and November 2020. The etiology of the heart failure in the patient group was idiopathic dilated cardiomyopathy. The ventricular tissues were obtained from the right ventricular side of the interventricular septum. Biopsy specimens were subjected to immunohistochemical analysis.

AAV9 CONSTRUCTION AND VECTOR DELIVERY IN MICE. Short hairpin RNA (shRNA) targeted to mouse *Nmt2* was generated by cloning into pAAV-2xU6 vector.[17] pAAV-CMV vector was constructed by subcloning mouse *Nmt2* with an N-terminal FLAG tag.[17] To administer recombinant adeno-associated virus 9 (AAV9), 10^{11} genome-containing units per mouse were injected via the lateral tail vein.

CLICK CHEMISTRY FOR LABELING N-MYRISTOYLATED PROTEINS. For click metabolic labeling,[18,19] Click-iT myristic acid azide (Thermo Fisher Scientific) was introduced to the cell culture. After cells were lysed, protein was incubated with alkyne-agarose resin with 50% slurry by Click-iT protein enrichment technology. Trypsin-digested peptides were introduced to subsequent analysis.

LIQUID CHROMATOGRAPHY–TANDEM MASS SPECTROMETRY. Liquid chromatography–tandem mass spectrometry (LC-MS/MS) was performed using an Easy-nLC1000 system (Thermo Fisher Scientific) coupled to a Q Exactive mass spectrometer 1000 (Thermo Fisher Scientific). An ion target value for mass spectrometry (MS) was set to 10^6, tandem MS to 10^5, and the intensity threshold was set to 1.8×10^3.

PROTEOMICS DATA ANALYSIS. All raw data acquired from LC-MS/MS spectra were processed with Proteome Discoverer version 1.4. The amino acid sequences of the peptides were identified using MASCOT and Sequest-HT search engines against Rat database in the SwissProt and Uniprot. Scaffold 5 (Proteome Software, Inc) was used to report tandem MS-based peptide.[20] The label-free quantification of LC-MS/MS was applied to determine protein abundance in each sample by measuring the intensity of the corresponding MS spectrum features of the protein.[21] Data were exported from Scaffold for statistical analysis of the differences in mean intensities among multiple replicate samples.

RNA SEQUENCING. The total RNA isolated from the heart tissues was subjected to RNA sequencing.[22]

STATISTICAL ANALYSIS. All data are expressed as the mean ± SEM unless otherwise specified. The Shapiro-Wilk test was used to assess normality. The unpaired Student's *t*-test was performed for comparisons of values between 2 groups unless otherwise specified. One-way analysis of variance followed by Tukey's post hoc test for multiple pairwise comparisons was applied when more than 2 groups were evaluated. Survival time was analyzed using Kaplan-Meier methods with the log-rank test used to compare groups. Data were analyzed using Statistical Package for Social Sciences version 28.0 (SPSS Inc) and GraphPad Prism version 9.5.1 (GraphPad Software).

ETHICAL APPROVAL. All animal studies were reviewed and approved by the Fukushima Medical University Animal Research Committee (approval number 2021129). The protocols involving human participants were approved by the institutional ethics committee of Fukushima Medical University Hospital (approval number 2020-309). The investigation conforms with the principles outlined in the Declaration of Helsinki.

RESULTS

ALTERATION OF CARDIAC NMT2 EXPRESSION DURING THE DEVELOPMENT OF HEART FAILURE. To clarify the role of NMTs in the development of heart failure, we first examined the changes in expression levels of NMT1 and NMT2, which are involved in N-myristoylation[8] in pathologically failing myocardium. In a murine model of heart failure induced through TAC using a 28-gauge blunt needle, which causes reduced left ventricular systolic function with left ventricular enlargement (Supplemental Table 1),[15,17] we observed that the protein levels of cardiac NMT1 were not significantly altered, whereas NMT2 protein levels were decreased by 59% at 4 weeks post-TAC in comparison to a control group that underwent sham surgery (**Figure 1A**). Likewise, immunohistochemical analysis demonstrated that NMT2 but not NMT1 represented a significant decrease in the failing heart (**Figures 1B and 1C**). When we assessed the human endomyocardial biopsy specimens from patients with symptomatic stage C/D heart failure with idiopathic dilated cardiomyopathy with left ventricular ejection fraction of 27.4% ± 16.4%, immunohistochemistry revealed that NMT2-expressing cardiomyocytes in patients with heart failure were significantly decreased compared to those without, whereas no difference in NMT1 expression was found between the 2 groups (**Figures 1D and 1E**, Supplemental Table 2). Alteration of cardiac NMT2 expression under pathological conditions suggests that NMT2 may participate in stress-induced cardiac remodeling and heart failure, as opposed to NMT1.

FIGURE 1 Changes in Cardiac NMT2 Expression in Heart Failure of Mice and Humans

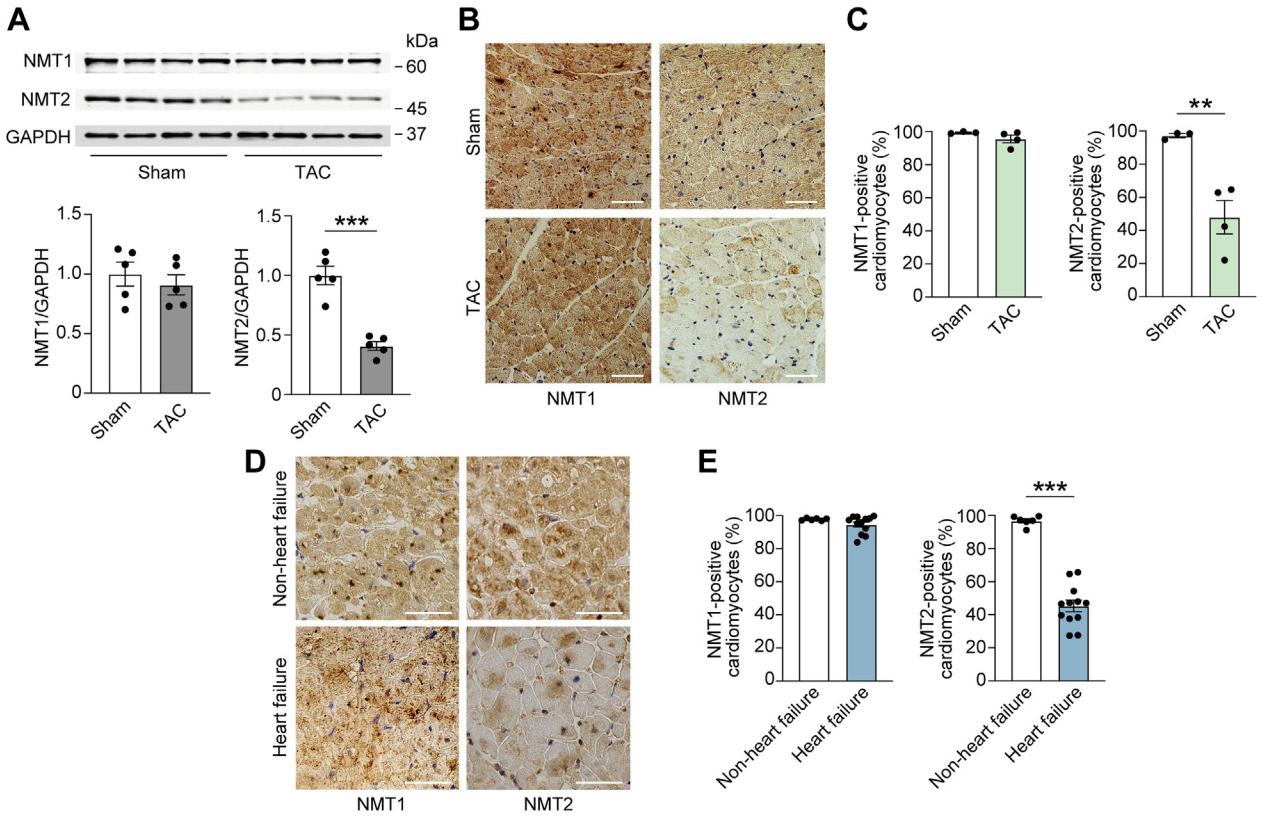

(A) Immunoblot analysis of N-myristoyltransferase 1 (NMT1) and N-myristoyltransferase 2 (NMT2) in the murine heart. Wild-type mice were subjected to either sham procedure or transverse aortic constriction (TAC) surgery using a 28-gauge blunt needle and analyzed 4 weeks after the operation. Glyceraldehyde-3-phosphate dehydrogenase (GAPDH) served as the loading control. The densitometric analysis is shown in the graphs (n = 5 in each). (B) Immunohistochemistry for NMT1 (brown) and NMT2 (brown) in paraffin-embedded sections from mouse hearts. Scale bars = 20 μm. (C) Quantitative analysis of the ratios of NMT1- or NMT2-positive cardiomyocytes determined by immunohistochemistry (n = 3 and 4, respectively). (D) Immunohistochemical analysis of NMT1 (brown) and NMT2 (brown) in paraffin-embedded heart section from non-heart failure control subjects and heart failure patients with idiopathic dilated cardiomyopathy. Scale bars = 20 μm. (E) Quantitative analysis of the ratios of NMT1- or NMT2-positive cardiomyocytes by immunohistochemistry (n = 6 and 12, respectively). All data are presented as mean ± SEM. $^{**}P < 0.01$ and $^{***}P < 0.001$ by the unpaired Student's *t*-test (2-sided).

NMT2 KNOCKDOWN IS MALADAPTIVE IN A MOUSE MODEL OF PATHOLOGICAL CARDIAC HYPERTROPHY AND FAILURE. To elucidate the role of N-myristoylation and endogenous NMT2 in the development of heart failure in vivo, we generated AAV9 vector encoding shRNA targets to NMT2 to inhibit NMT2 expression specific to the cardiomyocytes of mice.[17,23] To achieve the desired knockdown, we packed the separate loops for the 2 shRNAs from 2 U6 promoters of mU6 and hU6 into a single adeno-associated virus plasmid (Supplemental Figure 1). We administered a single dose of 1.0×10^{11} genome-containing units to the mice via the lateral tail vein at the age of 6 weeks (**Figure 2A**). After 3 weeks, the gene delivery of AAV9-shNMT2 was sufficient to elicit significant transduction and knockdown of NMT2 protein levels with a 58% decrease in the left ventricles compared to those injected with AAV9 encoding 2 shRNA against LacZ as a control (AAV9-ShCTRL) (Supplemental Figure 2) but did not affect NMT2 expression levels in the lung, liver, or anterior tibialis muscles (Supplemental Figure 3). We subjected the mice receiving AAV9-shNMT2 or AAV9-shCTRL injections to pressure overload-induced cardiac hypertrophy and failure by means of TAC using a 27-gauge blunt needle. Echocardiographic measurements revealed no cardiac physiological functional differences between AAV9-shNMT2- and AAV9-shCTRL-injected sham-operated mice followed by 4 weeks (Supplemental Table 3). Cardiac NMT2 expressions were reduced in both AAV9-shNMT2-injected sham- and TAC-operated mice compared to

FIGURE 2 **NMT2 Knockdown Is Maladaptive in a Mouse Model of Pathological Cardiac Hypertrophy and Failure**

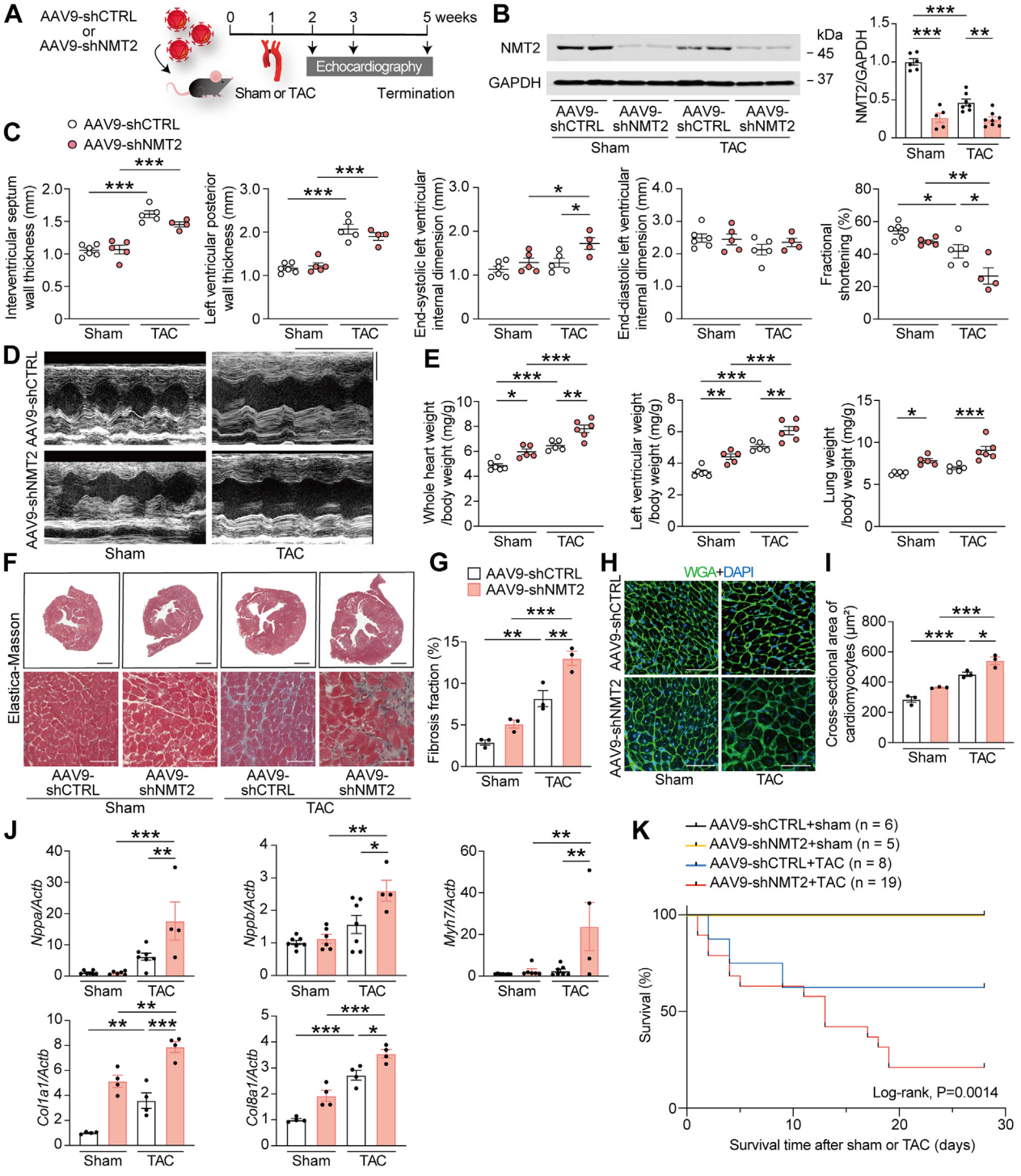

Continued on the next page

the corresponding AAV9-CTRL mice 4 weeks after operations (**Figure 2B**). Pressure overload triggered increases in end-diastolic interventricular septum wall thickness (IVSd) and end-diastolic left ventricular posterior wall thickness in both AAV9-shCTRL and AAV9-shNMT2 mice compared to the corresponding sham-operated mice at 1, 2, and 4 weeks post-operation (**Figures 2C and 2D**, Supplemental Table 3). There was no statistical significance on the degree of pressure overload according to the pressure gradient between AAV9-shCTRL and AAV9-shNMT2 mice at 1 week post-TAC (Supplemental Table 3). Importantly, TAC significantly reduced fractional shortening in AAV9-shCTRL mice at 2 and 4 weeks postsurgery; however, fractional shortening was significantly reduced in AAV9-shNMT2 mice compared to AAV9-shCTRL mice. Moreover, the end-systolic left ventricular internal dimension was larger in AAV9-shNMT2 mice than in AAV9-shCTRL mice after TAC. Although TAC enhanced whole heart weight and left ventricular weight-to-body weight ratios, these ratios were much higher in AAV9-shNMT2 mice than in AAV9-shCTRL mice (**Figure 2E**). Lung weight-to-body weight ratio, a measure of lung congestion, was elevated in TAC-operated AAV9-shNMT2 mice compared to TAC-operated AAV9-shCTRL mice. Elastica-Masson staining revealed that interstitial fibrosis in both AAV9-shCTRL and AAV9-shNMT2 mice was promoted by TAC compared to the corresponding sham-operated mice, although the extent of fibrosis in AAV9-shNMT2 mice was greater than in AAV9-shCTRL mice (**Figures 2F and 2G**). The cross-sectional area of cardiomyocytes according to the wheat germ agglutinin staining was substantially larger in TAC-operated AAV9-shNMT2 mice than in TAC-operated AAV9-shCTRL mice (**Figures 2H and 2I**). Messenger RNA (mRNA) expression levels of *Nppa*, *Nppb*, and *Myh7*, which are biochemical markers for cardiac remodeling and hypertrophy, as well as *Col1a1* and *Col8a1*, which are markers for fibrosis, were expressed at higher levels in AAV9-shNMT2 mice than in AAV9-shCTRL mice in response to TAC (**Figure 2J**). The total left ventricular mass, cardiomyocyte cell surface area, and gene expressions may not always correlate with changes in wall thickness measured by echocardiography, and the enhanced ventricular remodeling may have contributed to the nondetection of an increase in the thickness of IVSd in TAC-operated AAV9-shNMT2 mice. In addition, AAV9-shNMT2 hearts exhibited significant increases in the numbers of $CD45^+$ leukocytes and $CD68^+$ macrophages, as well as mRNA expression levels of *Il1b* compared to AAV9-shCTRL hearts atter TAC (Supplemental Figure 4). Some of TAC-operated AAV9-shNMT2 mice manifested conspicuous indications of cardiorespiratory distress, including decreased activity, reduced appetite, and piloerection, all of which are signs of heart failure, and when AAV9-shNMT2-injected mice were found dead, we observed congestive lungs in the mice. Noticeably, the mice receiving AAV9-shNMT2 injections followed by TAC demonstrated lower survival rates (**Figure 2K**). Sham-operated AAV9-shNMT2 mice exhibited increased heart weight and lung weight but did not lead to reduced left ventricular systolic function or survival during the 4-week observation period. These findings imply that NMT2 plays a crucial role in pressure overload-induced cardiac remodeling, heart failure, and survival.

GLOBAL PROFILING OF N-MYRISTOYLATED SUBSTRATES IN CARDIAC MYOCYTES BY CLICK CHEMISTRY–BASED QUANTITATIVE PROTEOMICS. To determine the global N-myristoylated protein profiling in cardiac myocytes, we applied an emerging click chemistry-based

FIGURE 2 Continued

(A) A schematic diagram of the experimental design. The mice at the age of 6 weeks were injected with 1.0×10^{11} genome-containing units of adeno-associated virus 9 (AAV9) encoding short hairpin RNA (shRNA) target to NMT2 (AAV9-shNTM2) or LacZ as a control (AAV9-shCTRL). One week later, TAC surgery using a 27-gauge blunt needle or sham procedure was performed. (B) Immunoblot analysis for NMT2 in the heart. The protein extracts from the left ventricles in mice receiving either AAV9-shCTRL or AAV9-shNMT2 at 4 weeks after sham or TAC operation were immunoblotted with the indicated antibodies. GAPDH was used as the loading control. The densitometric analysis is shown in the graphs (n = 5-8 in each group). (C) Echocardiographic assessment. Sham-operated AAV9-shCTRL–injected mice (n = 6), sham-operated AAV9-shNMT2–injected mice (n = 5), TAC-operated AAV9-shCTRL–injected mice (n = 5), and TAC-operated AAV9-shNMT2–injected mice (n = 4). (D) Representative images of M-mode echocardiograms. Scale bars = 0.2 seconds and 2 mm, respectively. (E) Physiological parameters. (F) Elastica-Masson–stained sections of the left ventricles. Scale bar = 1 mm (top) and 20 μm (bottom). (G) Quantitative analysis for fibrosis fraction in Elastica-Masson–stained sections (n = 3 in each). (H) Wheat germ agglutinin (WGA)-stained sections from the left ventricles. The plasma membrane and nucleus are stained with WGA (green) and 4′,6-diamidino-2-phenylindole (DAPI) (blue), respectively. Scale bar = 20 μm. (I) Quantification of the cross-sectional area of cardiomyocytes in WGA-stained sections (n = 3 in each). (J) Messenger RNA expressions of *Nppa*, *Nppb*, *Myh7*, *Col1a1*, and *Col8a1*. *Actb* was used for normalization. The average value for sham-operated AAV9-shCTRL–injected mice was set equal to 1 (n = 4-6). (K) Kaplan-Meier survival curve in AAV9-shCTRL– or AAV9-shNMT2–injected mice after sham or TAC surgery. The numbers of mice and *P* value by the log-rank test are presented. All data are presented as mean ± SEM. $*P < 0.05$, $**P < 0.01$, and $***P < 0.001$ by 1-way analysis of variance with Tukey's post hoc analysis. Abbreviations as in **Figure 1**.

FIGURE 3 **Global Profiling of Substrate Proteins of N-Myristoylation in Cardiac Myocytes by Click Chemistry–Based Quantitative Proteomics**

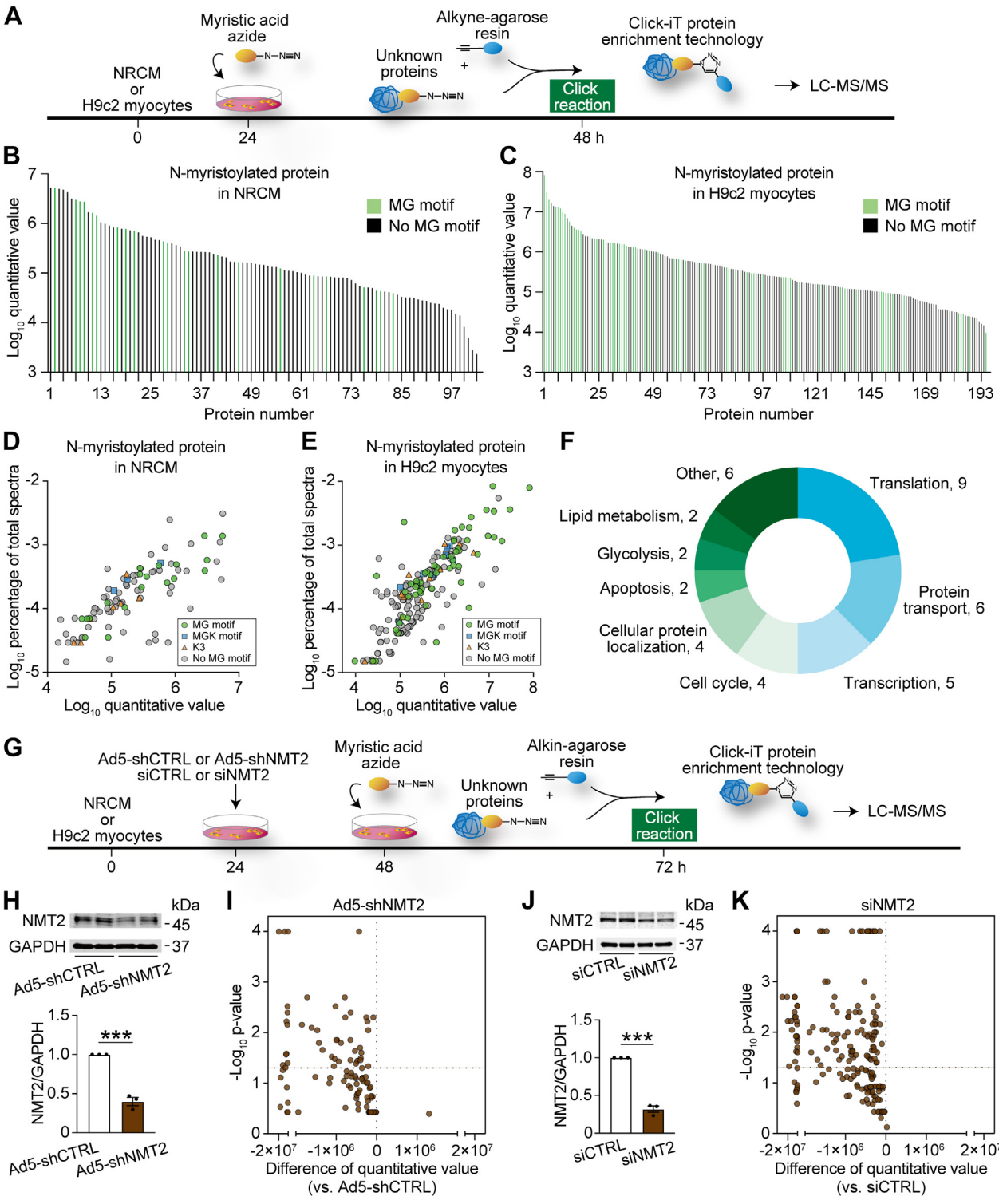

Continued on the next page

approach[24] in cultured neonatal rat cardiomyocytes (NRCMs) and H9c2 rat ventricular myocytes[25,26] (**Figure 3A**). The use of clickable fatty acids tagged with an alkyne or azide moiety has enabled the large-scale analysis of proteins as well as the discovery of new proteins by the purification of proteins labeled with lipid chemical reporters.[24] Cotranslationally, N-myristoylated proteins are generated continuously through de novo protein synthesis.[27] Proteins in the cells were labeled with click myristic acid azide, and then the azide-labeled N-myristoylated proteins were specifically captured for liquid chromatography-mass spectrometry-based proteomics analysis. Using the quantitative proteomics analysis followed by click chemistry, we identified 103 and 195 N-myristoylated-enriched proteins in NRCM and H9c2 myocytes, respectively (**Figures 3B and 3C**). Because N-terminal glycine residue (G2) is thought to constitute a degron that is N-myristoylated as an annotated N-terminal "MG" motif,[8] 22 and 65 proteins carried the N-terminal glycine, respectively (**Figures 3D and 3E**). Given that the occurrence of N-terminal lysine (K3) has been recently identified,[28] we observed that 3 and 8 proteins constituted the N-terminal "MGK" motif, and 7 and 12 proteins carried the N-terminal "K3" motif, respectively. The remaining 71 and 110 substrates were identified for the N-myristoylated substrates for the first time at the endogenous level in cardiac myocytes, respectively. We identified 40 N-myristoylated substrate proteins that are commonly present in NRCM and H9c2 cardiac myocytes. These proteins were categorized based on their biological functions using gene ontology annotation,[29] revealing their distribution across a variety of biological processes (**Figure 3F**), and the majority of N-myristoylated proteins were functionally associated with translation, protein transport, transcription, cell cycle, and cellular protein localization.

Next, to determine the involvement of NMTs in N-myristoylation in the myocytes, genetic inhibition by NMTs was applied (**Figure 3G**), rather than chemical inhibition or knockout considering the lethality of NMT knockouts.[30] For NRCM, adenovirus 5 with shRNA targeting to NMT2 was used to gain a significant knockdown of NMT2 (**Figure 3H**). Notably, NMT2 inhibition resulted in decreases in most of the N-myristoylated levels, and 44 of 103 N-myristoylated proteins exhibited a statistically significant reduction by inhibition of NMT2 (**Figure 3I**). Likewise, NMT2 inhibition reduced all N-myristoylation levels in H9c2 myocytes, and 110 of 195 N-myristoylated proteins represented a statistically significant reduction by NMT2 upon the knockdown conditions (**Figures 3J and 3K**). Together, we found that NRCM and H9c2 myocytes commonly contained 11 N-myristoylated proteins controlled by NMT2. Knockdown of NMT2 had no effects on the cell viability (Supplemental Figure 5). In contrast to NMT2, the majority of N-myristoylated levels were not significantly altered by the knockdown of NMT1 in H9c2 myocytes (Supplemental Figure 6).

ALTERATIONS OF N-MYRISTOYLATION LEVELS IN RESPONSE TO ANGIOTENSIN II IN CARDIAC MYOCYTES. We then employed the quantitative proteomics analysis with click chemistry following continuous angiotensin II (Ang II) stimulation[31] in combination with genetic knockdown of NMT2 to investigate the role of N-myristoylation during pathological cardiac hypertrophy and remodeling in the myocytes (**Figure 4A**). Of note, Ang II depressed the amounts of N-myristoylated levels in NRCMs, and 46 of 103 N-myristoylated proteins exhibited statistically significant attenuation in response to continuous Ang II stimulation (**Figure 4B**). Similarly, all N-myristoylated levels among these detected N-myristoylated

FIGURE 3 Continued

(A) A schematic diagram for the workflow of proteomic strategy using click chemistry. Neonatal rat cardiomyocytes (NRCMs) and H9c2 myocytes were incorporated with myristic acid azide for the labeling. N-myristoylated proteins were selectively captured by Click-iT protein enrichment technology using a click reaction with alkyne-agarose resin and analyzed by liquid chromatography–tandem mass spectrometry (LC-MS/MS). According to quantitative proteomics, 103 and 195 N-myristoylated-enriched proteins are identified in (B) NRCM and (C) H9c2 myocytes, respectively. The log quantitative value is plotted for each N-myristoylated substrate. The light green bars show proteins with the MG motif at the N-terminal, and the black bars show those with no MG motif. Data are presented as mean values from 5 and 3 independent experiments performed in triplicate, respectively. (D and E) Scatterplots for log quantitative value and log percentage of total spectra for N-myristoylated proteins according to the containing motif in (D) NRCM and (E) H9c2 myocytes. (F) Biological functions of 40 N-myristoylated proteins commonly detected in NRCM and H9c2 myocytes according to gene ontology annotation. (G) Chemical proteomic workflow with genetic inhibition of NMT2. NRCM were infected with Ad5-shNMT2 or LacZ (Ad5-shCTRL) at a multiplicity of infection of 100. H9c2 myocytes were transfected with small interfering RNA specific to NMT2 (siNMT2) or nontargeting control small interfering RNA (siCTRL). (H) Western blot analysis for NMT2 in NRCM infected with Ad5-shNMT2 for 48 hours ($n = 3$ in each). GAPDH was used as a loading control. The densitometric analysis is shown in the graph. (I) Volcano plots for N-myristoylated proteins in NRCM infected with Ad5-shNMT2 compared with those with Ad5-shCTRL from independent 3 experiments performed in triplicate. (J) Western blot analysis of NMT2 in H9c2 myocytes ($n = 3$ in each). (K) Volcano plots showing quantitative value and log *P* value for N-myristoylated proteins in H9c2 myocytes transfected with siNMT2 in comparison to siCTRL from independent 3 experiments performed in triplicate. ***$P < 0.001$ by the unpaired Student's *t*-test (2-sided). Abbreviations as in **Figures 1 and 2**.

FIGURE 4 Alteration in N-Myristoylated Levels in Response to Ang II in Cardiac Myocytes

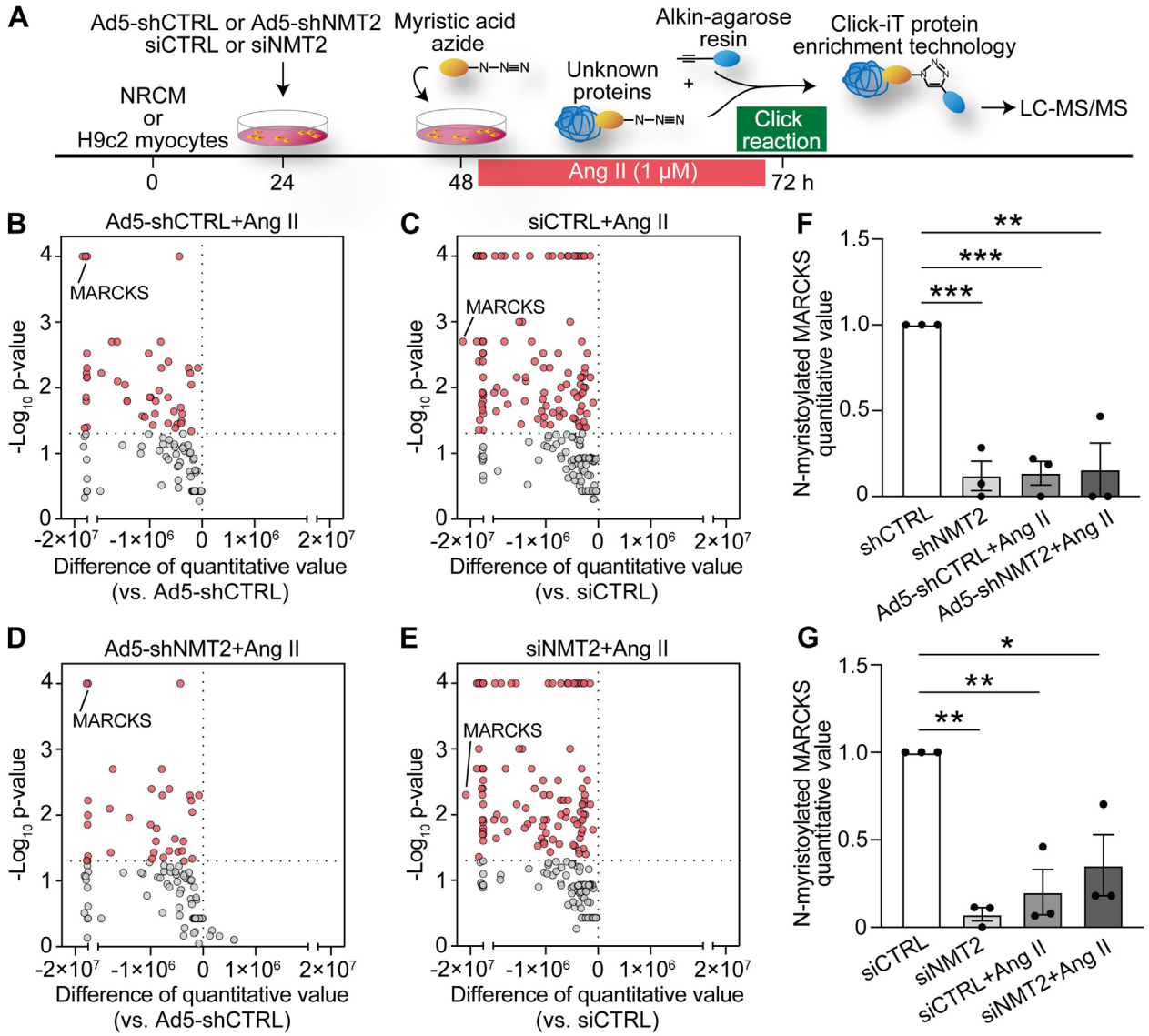

(A) The workflow for chemical proteomics. NMT2 expressions were inhibited in NRCM by Ad5-shNMT2 or in H9c2 myocytes by siNMT2, and then cells were stimulated with angiotensin II (Ang II, 1 μmol/L) for 24 hours before collection for click chemistry–based LC-MS/MS proteomics. (B to E) Volcano plots of the difference of quantitative value for N-myristoylated protein levels and log *P* value followed with the presence and absence of Ang II in Ad5-shCTRL- or Ad5-shNMT2–infected NRCM and in siCTRL- or siNMT2-transfected H9c2 myocytes from 3 independent experiments performed in triplicate. (F and G) Quantification of N-myristoylated MARCKS in (F) NRCM and (G) H9c2 myocytes. Data are presented as mean ± SEM (n = 3 in each). *$P < 0.05$, **$P < 0.01$, and ***$P < 0.001$ by 1-way analysis of variance with Tukey's post hoc analysis. Abbreviations as in Figures 1 to 3.

proteins were reduced, with 111 of 195 N-myristoylated showing a statistically significant reduction in response to Ang II in H9c2 myocytes (Figure 4C). Ang II treatment altered the protein expression levels of NMT2 but not NMT1 or cell viability (Supplemental Figures 7 and 8). NMT2 knockdown cells showed similar declining patterns of N-myristoylated levels following Ang II in comparison to the controls (Figures 4D and 4E). Among the identified N-myristoylated substrates, a unique protein, MARCKS, was found to be the most down-regulated N-myristoylated protein in H9c2 myocytes and the fourth most down-regulated in NRCM (Figures 4F and 4G). There was no change in MARCKS expression in Ang

II-treated or NMT2 knockdown H9c2 myocytes (Supplemental Figure 9). We estimated that MARCKS was a crucial component for N-myristoylation in Ang II-mediated pathological ventricular hypertrophy that is regulated by NMT2.

FUNCTIONAL ROLE OF N-MYRISTOYLATION OF MARCKS IN CARDIAC MYOCYTES. We next sought the functional significance of N-myristoylation of MARCKS in cardiac myocytes. MARCKS is known as an actin-binding protein that modulates cytoskeleton signaling and a substrate of protein kinase C to serve as a bridge between Ca^{2+}/calmodulin and protein kinase C signaling, which relate to cellular signal transduction.[32,33] The residue of N-terminus that is thought to be receiving N-myristoylation of MARCKS is highly conserved across species, including the MG motif (Supplemental Figure 10). The mutant MARCKS with replacement of N-terminal glycine to alanine ($MARCKS^{G2A}$) was generated to prevent N-myristoylation at the site. The immunofluorescence analysis demonstrated that wild-type MARCKS ($MARCKS^{WT}$) was localized to the cellular membrane, whereas $MARCKS^{G2A}$ was distributed throughout the cytoplasm in H9c2 myocytes (**Figures 5A and 5B**), indicating that N-myristoylation at N-terminal glycine facilitates the anchoring of MARCKS to the cellular membrane of the myocytes. Overexpression of $MARCKS^{WT}$ significantly reduced Ang II-induced cardiomyocyte hypertrophy (**Figures 5C and 5D**) followed by *Nppa*, *Nppb*, and *Myh7* mRNA expression (**Figure 5E**), whereas $MARCKS^{G2A}$ did not alter the cardiomyocyte surface area or these mRNA expression levels in H9c2 myocytes. To verify how N-myristoylation of MARCKS is implicated in Ang II-related cardiomyocyte hypertrophy, we assessed the involvement of Ca^{2+}/calmodulin-dependent protein kinase II (CaMKII), which is associated with cardiac hypertrophy induced by Ang II,[34,35] demonstrating that overexpression of $MARCKS^{WT}$ significantly inhibited Ang II-induced phosphorylation of CaMKII, whereas $MARCKS^{G2A}$ did not affect its phosphorylation levels (**Figure 5F**). Similarly, the impacts of $MARCKS^{WT}$ and $MARCKS^{G2A}$ on the activity of CaMKII during Ang II-mediated signal transduction were in accordance with the results from the phosphorylation of CaMKII (**Figure 5G**). MARCKS was not involved in PI3K/AKT pathway (Supplemental Figure 11). Acetylation of histones is a key epigenetic regulator and histone deacetylase 4 (HDAC4), a stress-responsive repressor, regulates cardiac gene expression by influencing calcium processing and activity of CaMKII.[36,37] Levels of phosphorylated HDAC4, as well as acetylated histone H3, were significantly elevated after Ang II treatment; however, $MARCKS^{WT}$ overexpression markedly reduced those levels, whereas $MARCKS^{G2A}$ overexpression did not change. These findings suggest that N-myristoylation of MARCKS plays a crucial role in Ang II-induced cardiac hypertrophy through CaMKII-related histone H3 acetylation via its localization at the plasma membrane.

ROLE OF NMT2 IN ANG II–INDUCED PATHOLOGICAL HYPERTROPHY IN CARDIAC MYOCYTES. We then studied the associations of NMT2 and cardiac hypertrophy during Ang II-mediated cardiac remodeling in H9c2 myocytes. NMT2 knockdown cells exhibited the absence of subcellular localization of $MARCKS^{WT}$ to the cellular membrane by immunofluorescence analysis, indicating that N-myristoylation-associated localization of MARCKS is regulated by NMT2 (**Figure 6A**). Cell surface area as well as mRNA expression levels of *Nppa*, *Nppb*, and *Myh7* increased in NMT2 knockdown cells, and Ang II-induced cardiac hypertrophy was accelerated in these cells (**Figures 6B to 6D**). This Ang II-related cardiac hypertrophy in NMT2-knockdown cells was accompanied by increases in phosphorylation of HDAC4 and acetylation of histone H3 (**Figure 6E**). Pharmacologic inhibition of CaMKII reduced Ang II-induced hypertrophic response in NMT2-knockdown H9c2 cardiac myocytes accompanied by decreasing levels of *Nppa*, *Nppb*, and *Myh7* mRNA expression as well as phosphorylation of HDAC4 and acetylation of H3 (**Figures 6F to 6I**), suggesting that the exacerbated hypertrophy by NMT2 knockdown is in part mediated by CaMKII. In contrast, transient overexpression of NMT2 significantly attenuated Ang II-induced cardiac hypertrophy as well as *Nppa*, *Nppb*, and *Myh7* mRNA expression accompanied by the reduction of HDAC4 phosphorylation and histone H3 acetylation in H9c2 myocytes (**Figures 6J to 6M**).

MARCKS N-MYRISTOYLATION–RELATED SIGNALING AND ITS INTRACELLULAR LOCALIZATION DURING PRESSURE OVERLOAD–INDUCED HEART FAILURE IN MICE. Based on our findings that N-myristoylation of MARCKS is a key during cardiomyocyte hypertrophy and remodeling in vitro, we sought to further investigate the downstream pathways regulated by NMT2 depletion in adult mouse myocardium. Western blotting analysis revealed that hearts with AAV9-mediated NMT2 knockdown represented increased levels of phosphorylated CaMKII and HDAC4 phosphorylation (**Figure 7A**) as well as acetylated H3 (**Figure 7B**) at 4 weeks post-TAC. Although the total levels of MARCKS expression did not vary significantly across the groups (Supplemental Figure 12), MARCKS expression in the plasma membrane fraction

FIGURE 5 Functional Role of N-Myristoylation of MARCKS in Cardiac Myocytes

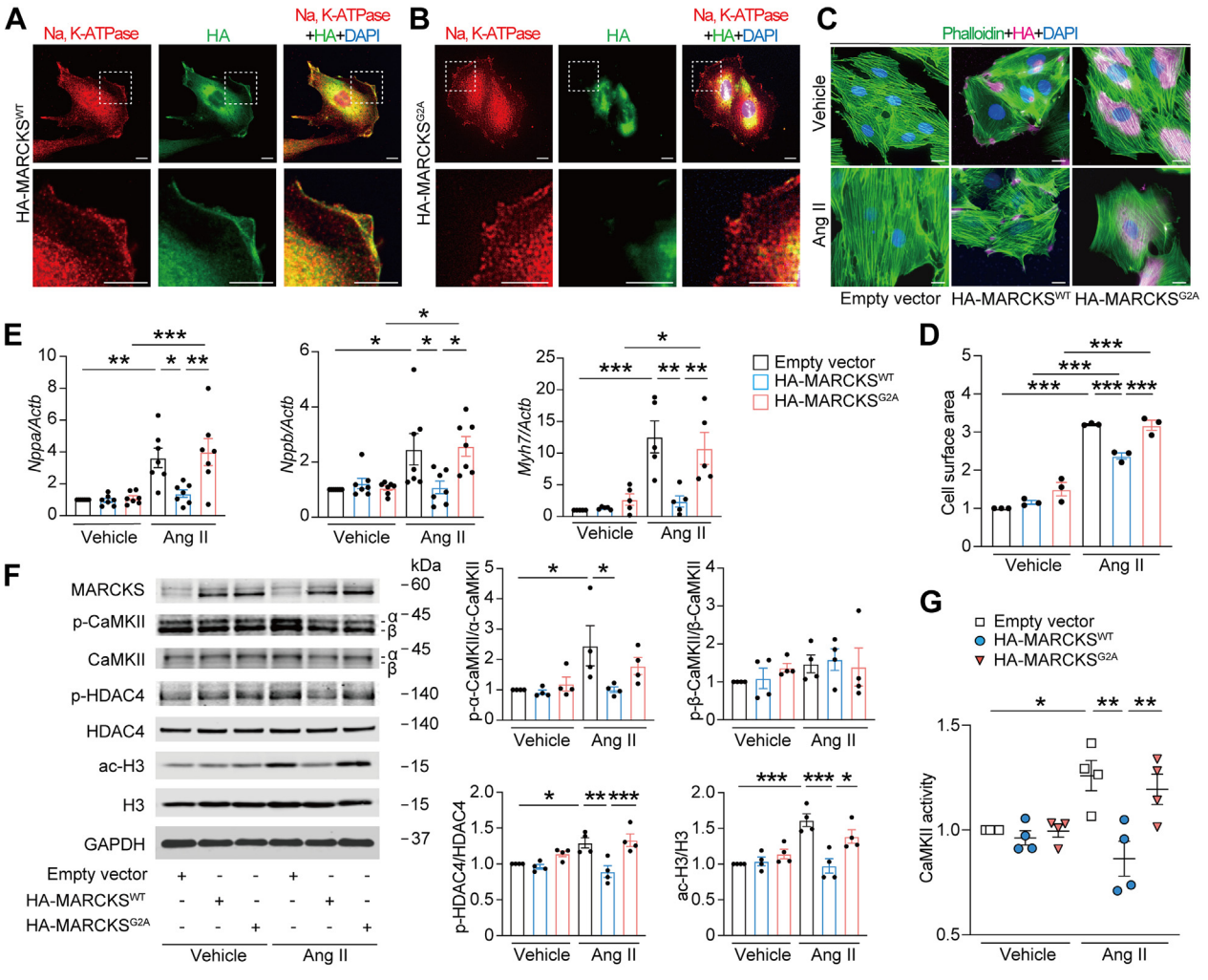

(A and B) Immunofluorescence images for subcellular localization of MARCKS. H9c2 myocytes were transfected with hemagglutinin (HA)-tagged wild-type MARCKS (MARCKS^{WT}) or HA-tagged mutant MARCKS with replacement of N-terminal glycine to alanine (MARCKS^{G2A}) for 48 hours. Cells were stained with anti-Na, potassium-adenosine triphosphatase (K-ATPase) (red), and anti-HA (green) antibodies with DAPI (blue). Images in boxed areas at higher magnification are shown in lower panels. Scale bars = 5 μm. (C) Immunofluorescence images for assessment of myocyte hypertrophy. Transfected H9c2 myocytes with empty vector, MARCKS^{WT}, or MARCKS^{G2A} were stimulated with vehicle or Ang II (1 μmol/L) for 24 hours and stained with phalloidin (green), anti-HA (magenta) antibody, and DAPI (blue). Scale bar = 5 μm. (D) Quantitative analysis of the cell surface area determined by phalloidin staining. Data are expressed as a relative ratio to empty vector with vehicle from 3 independent experiments. (E) Messenger RNA expression levels in *Nppa*, *Nppb*, and *Myh7*. The data were normalized to *Actb* levels (n = 5-7 in each). (F) Immunoblot analysis for Ca^{2+}/calmodulin-dependent protein kinase II (CaMKII) phosphorylation, histone deacetylase 4 (HDAC4) phosphorylation, and histone H3 acetylation in H9c2 myocytes. The ratios of phosphorylated α-CaMKII (p-α-CaMKII) to total α-CaMKII, phosphorylated β-CaMKII (p-β-CaMKII) to total β-CaMKII, phosphorylated HDAC4 (p-HDAC4) to total HDAC4, and acetylated H3 (ac-H3) to total H3 are quantified and presented in the graphs (n = 4 in each). (G) CaMKII activity. Forty-eight hours after transfection followed by Ang II, cell lysates were collected, and activities of CaMKII were determined and expressed as a relative ratio over the control group of empty vector with vehicle (n = 4 in each). All data are presented as mean ± SEM. *$P < 0.05$, **$P < 0.01$, and ***$P < 0.001$ by 1-way analysis of variance with Tukey's post hoc analysis.

was significantly decreased in response to TAC, and NMT2-knockdown hearts showed a significant reduction in the membranous MARCKS expression compared with AAV9-shCTRL hearts after TAC (**Figure 7C**). MARCKS expression was likely to be distributed in the plasma membrane of cardiomyocytes in individuals without heart failure, whereas it was not clearly present at the plasma membrane of cardiomyocytes in patients with heart failure (Supplemental Figure 13). These findings suggest that N-myristoylation by NMT2 anchors MARCKS at the cellular membrane, and the protective

FIGURE 6 Role of NMT2 in Ang II–Induced Pathological Hypertrophy

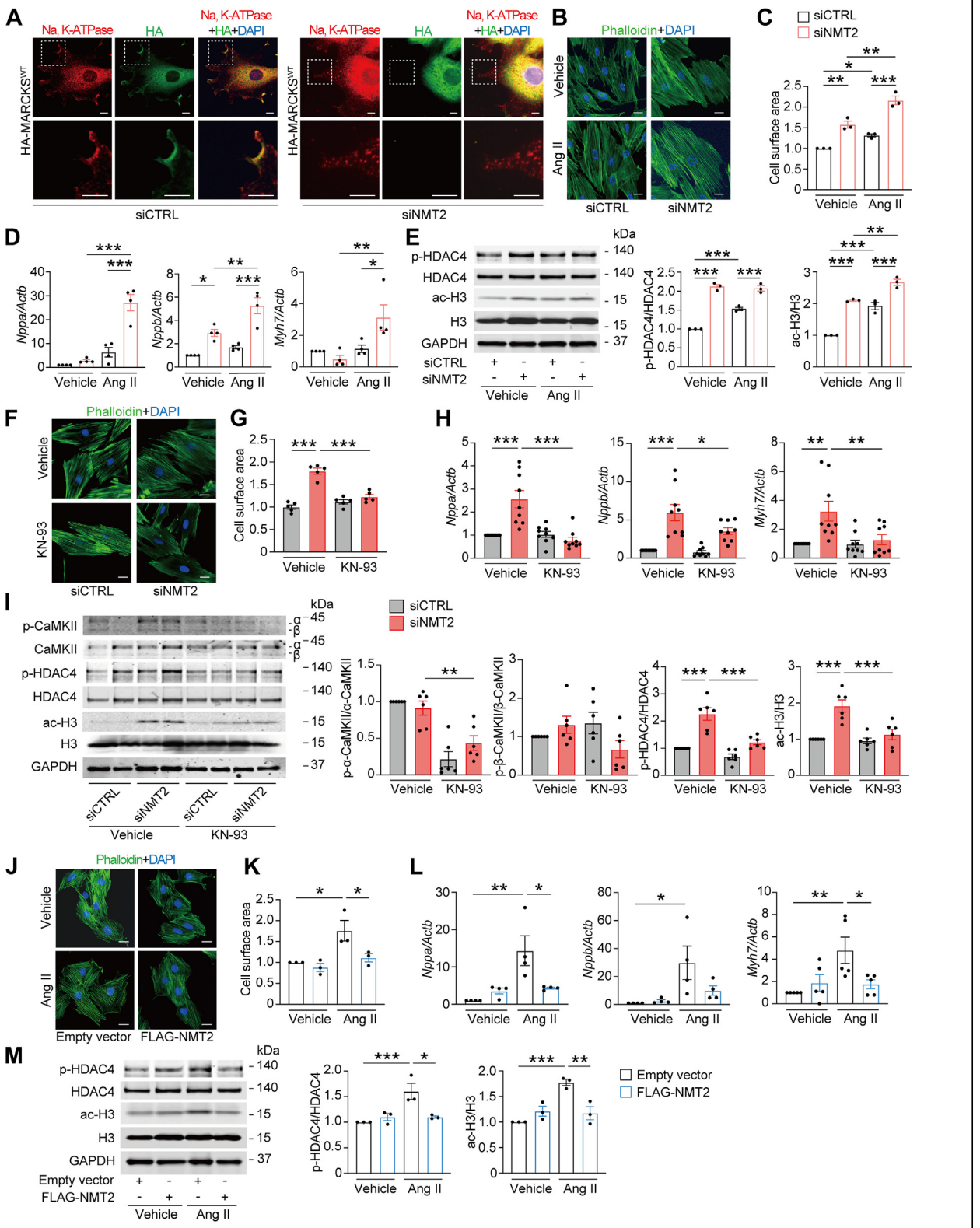

Continued on the next page

effects of NMT2 are mediated through CaMKII-related acetylation of histone H3.

NMT2 GENE TRANSFER SPECIFIC TO THE HEART PREVENTS CARDIAC PATHOLOGICAL HYPERTROPHY AND REMODELING IN A MURINE MODEL OF HEART FAILURE. Given that loss of function of NMT2 was maladaptive, we sought to clarify whether NMT2 gain of function could attenuate cardiac remodeling in mice and whether AAV9-mediated gene therapy could be a potential approach. Accordingly, recombinant AAV9 encoding mouse NMT2 with a FLAG tag (AAV9-NMT2) specific to the heart was generated (**Figure 8A**, Supplemental Figure 14). After a single dose of injection of AAV9-NMT2 with 1.0×10^{11} genome-containing units, the immunofluorescence analysis showed the ratios of FLAG-positive cardiomyocytes in the left ventricles to estimate the transduction efficiency was 63.7% at 4 weeks, and FLAG-NMT2 was likely to localize to the cytoplasm in the cardiomyocytes (**Figure 8B**). At the protein levels, left ventricular NMT2 expression indicated 2.9 times increase compared to endogenous NMT2 levels by immunoblotting (Supplemental Figure 15). NMT2 expression levels in the lung, liver, and anterior tibialis muscles were not different between AAV9-NMT2 mice and AAV9-CTRL mice (Supplemental Figure 16). Then, the mice receiving AAV9-NMT2 or AAV9 encoding LacZ as a control (AAV9-CTRL) injections were subjected to TAC using a 28-gauge blunt needle, and more severe constriction to the transverse aorta was applied to achieve the enhanced cardiac dysfunction and failure for the wild-type mice in this series.[16] TAC decreased cardiac NMT2 expression levels, but AAV9-mediated NMT2 gene delivery significantly increased them in TAC-operated mice (**Figure 8C**). Echocardiographic analysis revealed that IVSd and left ventricular posterior wall thickness in AAV9-NMT2 mice were lower than in AAV9-CTRL mice at 2 and 4 weeks after TAC (**Figures 8D and 8E**, Supplemental Table 4). Of note, TAC significantly decreased fractional shortening in AAV9-CTRL mice at 1, 2, and 4 weeks, but the cardiac systolic function was preserved in TAC-operated AAV9-NMT2 mice compared to TAC-operated AAV9-CTRL mice. The left ventricular dilation was prevented in AAV9-NMT2 mice according to the end-diastolic left ventricular internal dimension at 4 weeks post-TAC. Whole heart weight- and left ventricular weight-to-body weight ratios were much lower in TAC-operated AAV9-NMT2 mice than in TAC-operated AAV9-CTRL mice (**Figure 8F**). Furthermore, the severe pressure overload caused lung congestion, whereas the lung weight-to-body weight ratio was significantly lower in TAC-operated AAV9-NMT2 mice than in TAC-operated AAV9-CTRL mice. The fibrosis fraction and cross-sectional area of cardiomyocytes were significantly reduced in AAV9-NMT2 mice comparing AAV9-CTRL mice after TAC (**Figures 8G to 8J**). Correspondingly, mRNA expression levels in *Nppa*, *Nppb*, and *Myh7* as well as *Col1a1* and *Col8a1* were lower in TAC-operated AAV9-NMT2 mice than in TAC-operated AAV9-CTRL mice (**Figure 8K**). The numbers of $CD45^+$ leukocytes and $CD68^+$ macrophages in AAV9-NMT2 hearts were significantly decreased compared to AAV9-CTRL hearts after TAC (Supplemental Figure 17). These findings indicate

FIGURE 6 Continued

(A) Representative immunofluorescence images for localization of MARCKS in H9c2 myocytes. Twenty-four hours after transfection with siCTRL or siNMT2, HA-$MARCKS^{WT}$ was transfected and stained for anti-Na, K-ATPase (red), and anti-HA (green) antibodies with DAPI (blue). Images in boxed areas at higher magnification are shown in lower panels. Scale bars = 5 μm. (B) Immunofluorescence images for the assessment of myocyte hypertrophy altered by the inhibition of NMT2. Transfected H9c2 myocytes with siCTRL or siNMT2 were stimulated with vehicle or Ang II (1 μmol/L) for 24 hours and stained with phalloidin (green) and DAPI (blue). Scale bars = 5 μm. (C) Quantitative analysis of the cell surface area determined by phalloidin staining. More than 100 cells were counted. Data are expressed as a relative ratio over siCTRL with vehicle from 3 independent experiments. (D) Messenger RNA expression levels in *Nppa*, *Nppb*, and *Myh7*. The data were normalized to *Actb* levels (n = 4 in each). (E) Western blot analysis on HDAC4 phosphorylation and histone H3 acetylation. Quantitative analyses of the ratios of phosphorylated HDAC4 (p-HDAC4) to total HDAC4 and acetylated H3 (ac-H3) to total H3 are shown in the graphs (n = 3 in each). (F) Involvement of CaMKII-related signaling in Ang II–induced hypertrophic response in NMT2-knockdown H9c2 myocytes. siRNA-transfected cells were incubated with CaMKII inhibitor (KN-93, 5 μmol/L) or vehicle for 1 hour before Ang II (1 μmol/L) stimulation. Twenty-four hours after Ang II, cell surface area was assessed by phalloidin (green) and DAPI (blue) staining. Scale bar = 5 μm. (G) Quantitative analysis of the cell surface area determined by phalloidin staining. Data are expressed as a relative ratio over siCTRL with vehicle from 5 independent experiments. (H) mRNA expression levels in *Nppa*, *Nppb*, and *Myh7*. The data were normalized to *Actb* levels (n = 9 in each). (I) Immunoblot analysis for phosphorylation of CaMKII and HDAC4 and acetylation of histone H3 (n = 6 in each). Data are expressed as a relative ratio over vehicle-treated siCTRL group. (J) Assessment of hypertrophic responses with overexpression of NMT2 by immunofluorescence. Transfected H9c2 myocytes with empty vector or FLAG-NMT2 were stimulated with vehicle or Ang II (1 μmol/L) for 24 hours and stained with phalloidin (green) and DAPI (blue). Scale bar = 5 μm. (K) Quantitative analysis of the cell surface area determined by phalloidin staining. Data are expressed as a relative ratio over empty vector with vehicle from 3 independent experiments. (L) Messenger RNA expression levels in *Nppa*, *Nppb*, and *Myh7*. The data were normalized to *Actb* levels (n = 4-5 in each). (M) Western blot analysis on HDAC4 phosphorylation and histone H3 acetylation (n = 3 in each). All data are presented as mean ± SEM. *$P < 0.05$, **$P < 0.01$, and ***$P < 0.001$ by 1-way analysis of variance with Tukey's post hoc analysis. Abbreviations as in **Figures 1 to 5**.

FIGURE 7 MARCKS N-Myristoylation–Related Signaling During Pressure Overload–Induced Heart Failure in Mice With AAV9-Mediated NMT2 Knockdown

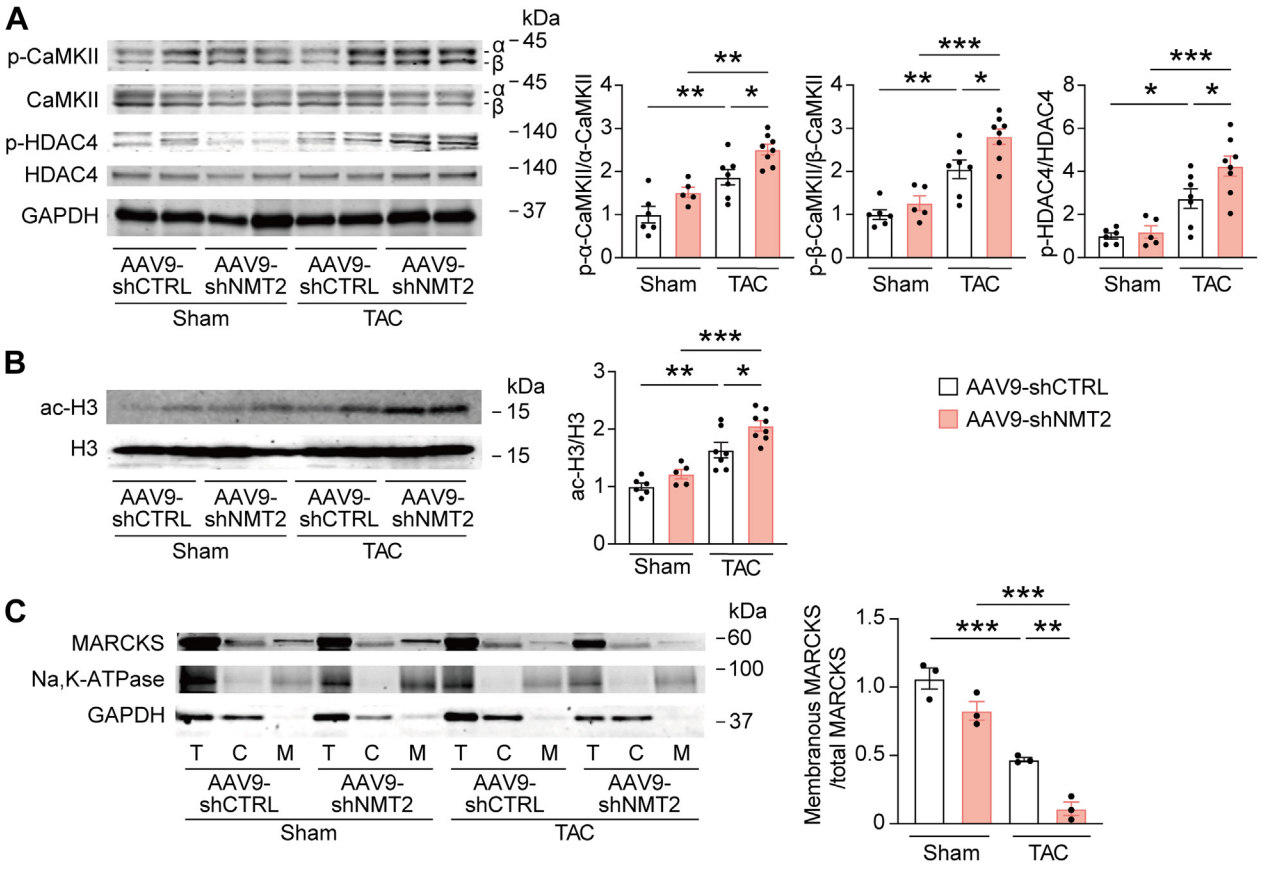

Immunoblot analysis for CaMKII phosphorylation, (A) HDAC4 phosphorylation and (B) histone H3 acetylation. The protein extracts from the left ventricles in mice receiving either AAV9-shCTRL or AAV9-shNMT2 at 4 weeks post-sham or -TAC operation were immunoblotted with the indicated antibodies. The ratios of p-α-CaMKII to total α-CaMKII, p-β-CaMKII to total β-CaMKII, p-HDAC4 to total HDAC4, and ac-H3 to total H3 are quantified and presented in the graphs (n = 5-8). GAPDH was used as the loading control. (C) Fractionated immunoblots for intracellular distribution of MARCKS in the hearts following AAV9-mediated NMT2 knockdown. The fractions are represented as membranous (M) and cytosolic (C). T represents a total protein. The levels of plasma membranous MARCKS were normalized to the total levels of MARCKS (n = 3 in each). Na, K-ATPase, and GAPDH were used as controls to ensure the quality of plasma membrane and cytoplasm fractionation, respectively. All data are presented as mean ± SEM. *$P < 0.05$, **$P < 0.01$, and ***$P < 0.001$ by 1-way analysis of variance with Tukey's post hoc analysis. Abbreviations as in Figures 1, 2, and 5.

that NMT2 gene transfer specific to the heart improves cardiac pathological hypertrophy and remodeling in response to pressure overload.

PROTECTIVE EFFECTS OF NMT2 IN THE HEART ARE MEDIATED BY CaMKII-RELATED HISTONE H3 ACETYLATION SIGNALING. To understand the mechanistic relevance of the protective effects of NMT2 in the heart, we assessed the downstream pathways regulated by NMT2 in adult mouse myocardium. Although pressure overload by TAC significantly up-regulated CaMKII phosphorylation and HDAC4 phosphorylation as well as H3 acetylation at 4 weeks postsurgery, the hearts with AAV9-mediated NMT2 overexpression showed significant decreases in phosphorylated CaMKII and HDAC4 (Figure 9A) as well as acetylated H3 (Figure 9B) compared to AAV9-CTRL-injected hearts. In contrast, MARCKS expression levels were not different among the groups (Supplemental Figure 18). According to the KEGG functional enrichment analysis pathways acquired by RNA sequence from the left ventricle, TAC-operated AAV9-NMT2 mouse hearts showed enhanced pathways including AMPK signaling, adrenergic signaling, and longevity regulating pathways in comparison to TAC-operated AAV9-CTRL mice (Figure 9C), suggesting that these pathways associated with N-myristoylation by NMT2 integrate a

FIGURE 8 **NMT2 Gene Transfer Specific to the Heart Prevents Cardiac Pathological Hypertrophy and Remodeling in a Murine Model of Heart Failure**

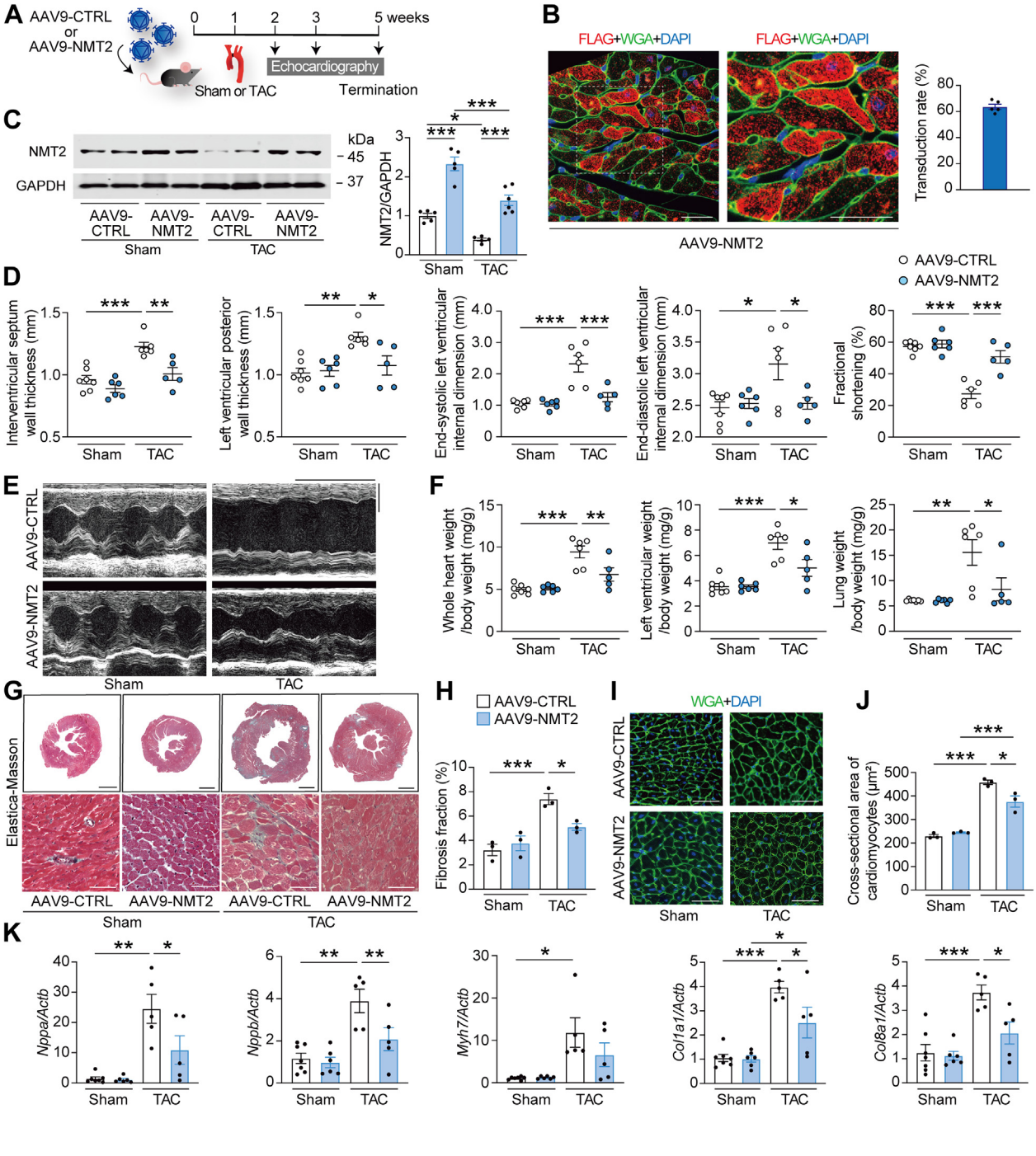

Continued on the next page

protective role in the development of heart failure (Figure 9D). In aggregates, our findings support a functional capacity of cardiac NMT2 in vivo to prevent pressure overload-induced hypertrophy and heart failure.

DISCUSSION

The present study is the first to demonstrate the key role of NMT2 in the development of heart failure and to identify the global profiling of substrate proteins of

N-myristoylation in cardiac myocytes through click chemistry-based quantitative proteomics. MARCKS was identified as a crucial N-myristoylation substrate regulated by NMT2 that controls cardiac remodeling and hypertrophic responses. Up-regulation of N-myristoylation by transferring NMT2 gene to the heart attenuated pressure overload-induced cardiac remodeling and heart failure.

PTMs have significant roles in signal transduction by controlling the localization and activity of proteins within the cells.[3,7] Among these modifications, lipid modification of proteins functions to increase the hydrophobicity of the substrate protein and localize it to the cell membrane or organelle membrane.[5] Recent chemical technologies of click chemistry allow selective labeling and enrichment of proteins for their identification and quantitation at the endogenous level in living cells when combined with proteomic techniques.[38] Using this system, the large-scale N-myristoylation mapping has been demonstrated in a cervical carcinoma cell line,[27] whereas we characterized N-myristoylated proteins in cardiac myocytes. H9c2 myocytes that are originally derived from ventricular tissue are now widely used as an alternative for cardiomyocytes in cardiac research.[25,26] When NMT activities were pharmacologically inhibited, HeLa cells demonstrated a clear distinction between cotranslational substrates and nonsubstrates of N-myristoylation.[27] In contrast, we applied genetic modification through NMT knockdown in the myocytes for targeting genetic therapeutic advantage in the current investigation. According to our data, 12 and 48 N-myristoylation substrates in NRCM and H9c2 myocytes, respectively, were identical to those in HeLa cells from the previous demonstration.[27] It has subsequently been found that certain lysine residues can be N-myristoylated in addition to glycine residue in the MG motif.[28] The discovery of certain N-myristoylated proteins in our study for the first time at the endogenous level in cardiac cells suggests protein diversity in N-myristoylation modification and the need for further investigation into the functional effects of each protein. It is likely that N-myristoylation is predominantly regulated by NMT2 rather than NMT1 in cardiac myocytes. Although NMT1 and NMT2 have 3 identical myristoyl-coenzyme A binding sites, NMT2 is phosphorylated at the Ser38 residue NMT2, whereas NMT1 can be phosphorylated at Ser31, Ser47, and Ser83.[39] It remains clarified how NMT activation differs across cardiomyocytes and other types of cells.

MARCKS is reported to be a substrate of protein kinase C to connect Ca^{2+}/calmodulin, which relate to cellular adhesion, migration, and exocytosis.[40] We showed that N-myristoylation is essential for MARCKS to function through its localization to the plasma membrane in cardiac myocytes. Ang II generates phosphatidylinositol 4,5-bisphosphate (PIP_2)[35] and lipid second messengers that activate Ca^{2+}-dependent CaMKII. MARCKS at the plasma membrane binds to PIP_2 and controls the level of free PIP_2,[41] and we found that overexpression of $MARCKS^{WT}$ resulted in the inhibition of CaMKII activation and phosphorylation of HDAC4, subsequently leading to acetylation of histones during Ang II–associated cardiac hypertrophy. It is recently reported that the N-terminal fragment of HDAC4 protects the heart by decreasing NR4A1-dependent activation of the hexosamine biosynthetic pathway.[37] Accordingly, the failure to N-myristoylation of MARCKS did not prevent Ang II–induced phosphorylation of HDAC4 and acetylation of histones, which caused pathological cardiomyocyte hypertrophy. N-myristoylation of

FIGURE 8 Continued

(A) Experimental design. AAV9 encoding mouse NMT2 with a FLAG-tag (AAV9-NMT2) with 1.0×10^{11} genome-containing units were injected in mice at the age of 6 weeks. AAV9 encoding mouse LacZ was used as a control (AAV9-CTRL). One week later, TAC surgery using a 28-gauge blunt needle or sham procedure was performed. (B) Representative images of immunohistochemistry for FLAG (red) and wheat germ agglutinin (WGA) (green) with DAPI (blue) from left ventricular tissue sections 5 weeks after AAV9-NMT2 injections. Boxed areas are highlighted in the right panel. Scale bars = 20 μm. The transduction rate of AAV9-NMT2 in the left ventricles is presented in the graph according to the ratio of cardiomyocytes with FLAG-positives (n = 5). (C) Immunoblot analysis for NMT2 in the heart. (D) Echocardiographic parameters. Sham-operated AAV9-CTRL–injected mice (n = 7), sham-operated AAV9-NMT2–injected mice (n = 6), TAC-operated AAV9-CTRL–injected mice (n = 6), and TAC-operated AAV9-NMT2–injected mice (n = 5). (E) Representative images of M-mode echocardiograms. Scale bars = 0.2 seconds and 2 mm, respectively. (F) Physiological parameters. (G) Elastica-Masson–stained sections of the left ventricles. Scale bar = 1 mm (top) and 20 μm (bottom). (H) Quantitative analysis of fibrosis fraction in Elastica-Masson–stained sections (n = 3 in each). (I) Representative images of WGA (green)- and DAPI (blue)-stained sections. Scale bar = 20 μm. (J) Quantitative analysis for the cross-sectional area of cardiomyocytes from WGA-stained sections. More than 100 cardiomyocytes were analyzed (n = 3 in each). (K) Messenger RNA expression of *Nppa*, *Nppb*, *Myh7*, *Col1a1*, and *Col8a1* from the left ventricles by reverse transcription–quantitative polymerase chain reaction. *Actb* was used as the loading control. The average value for sham-operated AAV9-CTRL–injected mice was set equal to 1 (n = 5-7). All data are presented as mean ± SEM. $*P < 0.05$, $**P < 0.01$, and $***P < 0.001$ by 1-way analysis of variance with Tukey's post hoc analysis. Abbreviations as in Figures 1 and 2.

FIGURE 9 Protective Effects of NMT2 in the Heart Are Mediated by CaMKII-Related Histone H3 Acetylation Signaling

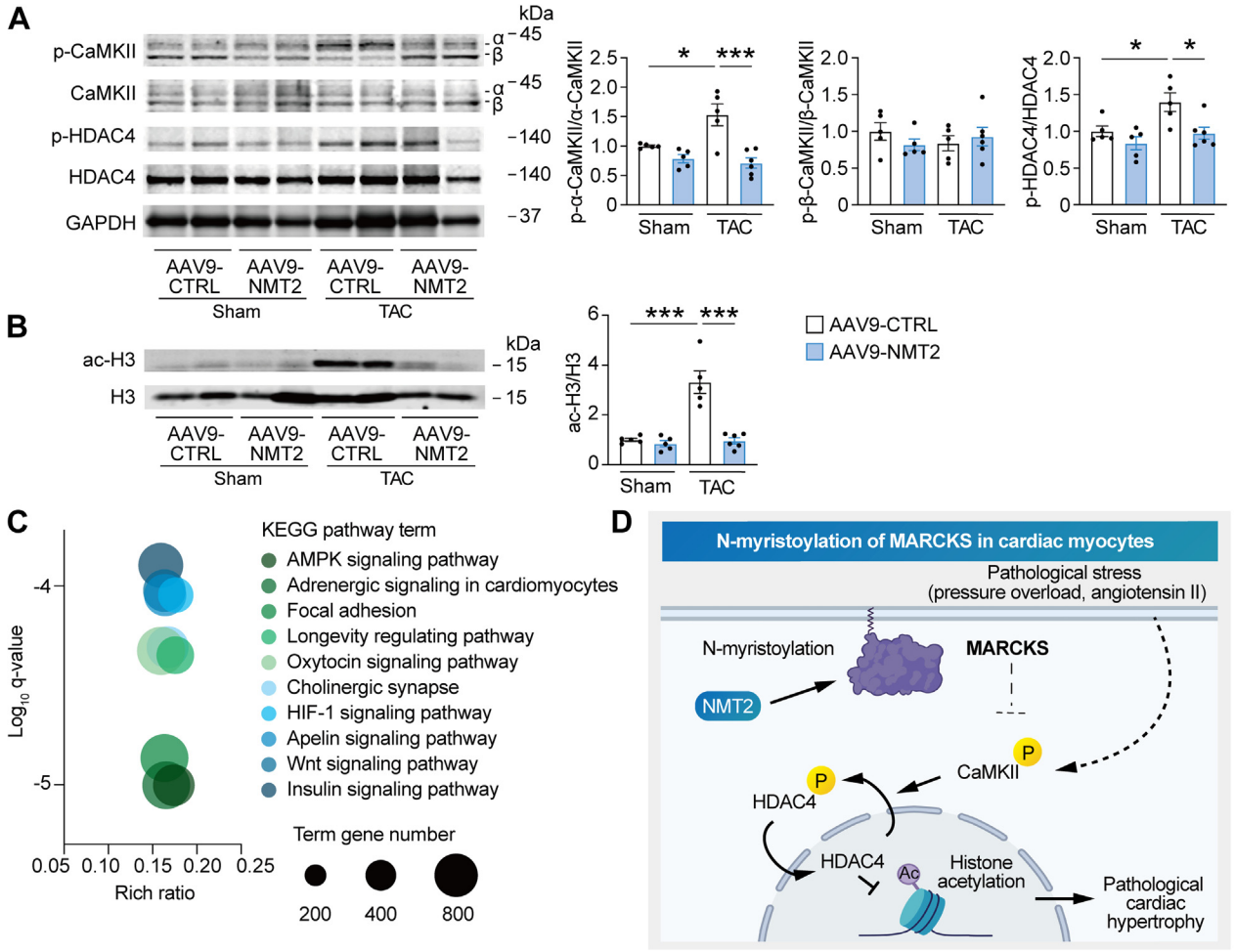

Immunoblot analysis for CaMKII phosphorylation, (A) HDAC4 phosphorylation, and (B) histone H3 acetylation in cardiac NMT2-overexpressing mice after TAC (n = 5-8). (C) KEGG analyses of RNA sequencing from the left ventricle. Log q-values, rich ratio, and top 10 KEGG enrichment pathways of TAC-operated mice receiving AAV9-NMT2 in comparison to TAC-operated AAV9-CTRL–injected mice are shown in a bubble plot. The size of the circle depicts the number of genes annotated to each KEGG pathway. (D) The proposed model of a cardioprotective role of N-myristoylation through NMT2 in cardiac myocytes. All data are presented as mean ± SEM. *$P < 0.05$ and ***$P < 0.001$ by 1-way analysis of variance with Tukey's post hoc analysis. Abbreviations as in Figures 1, 5, and 8.

MARCKS may be a significant molecular switch that determines the ability of a cardiomyocyte to adapt to physiological or pathological stress. In contrast, given that modulation of CaMKII and H3 acetylation could be an epiphenomenon and that H3 acetylation status is governed broadly by multiple histone acetyltransferases and histone deacetylases, we need to clarify a causal relationship between the MARCKS-CaMKII-HDAC4-H3 axis and Ang II-induced hypertrophy.

N-myristoylation is linked to various clinical diseases, which raises the possibility of a therapeutic approach. A point mutation in the MG motif of the *SHOC2* gene, which causes Noonan-like syndrome characterized by developmental disorder, results in abnormal N-myristoylation and altered localization of SHOC2 to the plasma membrane.[42] Given that NMT expression levels and activity were up-regulated, NMT inhibitors have been reportedly therapeutic targets for certain neoplasms such as B-cell lymphomas[13] and breast cancer.[43] Recently, N-myristoylation has been shown to play a role in N-terminal stability and protein stabilization involved in the novel N-end rule pathway specific to a glycine.[14] In cardiac myocytes, genetic inhibition of NMT2 did not affect the cell viability or cardiac

contractility but led to an increase in cardiac hypertrophy and had an impact on cardiomyocyte pathological hypertrophy and remodeling in response to specific stimuli. Compensated mechanisms may have played a role in preserving systolic cardiac function in AAV9-shNMT2 mice, and further investigation is required to clarify the cardiac phenotype in NMT2 knockdown in uninured mice over the long-term. N-myristoylation has been shown to play an important role in innate responses via its property in mediating the controlled localization of specific proteins to the cell membrane to interact with other innate mediators during signal transduction in immune cells.[44] Although the specific roles of N-myristoylation may vary between cell types, our data suggest that the activation of the immune system may be in part associated with the progression of left ventricular hypertrophy and cardiac dysfunction in NMT2-knockdown hearts.

AAV9-mediated gene therapy targeting NMT2 in the heart has the potential to modify N-myristoylation levels in cardiomyocytes. In failing hearts, proper membrane targeting and function of proteins may require N-myristoylation because this modification is considered irreversible and stable.[40] AAV9 has been shown to be the most efficient adeno-associated virus serotype for infection of cardiomyocytes within the heart.[45] Restoring N-myristoylation levels of MARCKS by exogenous NMT2 overexpression is critical for reversing pathological remodeling processes, although N-myristoylation of other myocardial targets than MARCKS may also contribute to the reversal of cardiac dysfunction. Gene transfer of MARCKS in combination with NMT2 may be more efficient for improving cardiac dysfunction, but our findings suggest that NMT2 gene therapy alone is sufficient to rescue the cardiac phenotypes. In addition to MARCKS, we have discovered unique N-myristoylated proteins such as GLIPR2[46] in cardiac cells that may be modified by NMT2 and have functional impacts on preventing cardiac remodeling and failure. Further study is needed to fully understand these proteins and their potential roles.

STUDY LIMITATIONS. A limitation of the current study is that the direct atlas of global N-myristoylation proteomes of the adult mouse or human heart was not determined because of the principle of click chemistry technology; therefore, further research needs to clarify the cardiomyocyte-specific proteomes using induced pluripotent stem cell-derived cardiomyocytes or adult cardiomyocytes derived from living animals. Although AAV9 preferably targets the heart, cardiac gene transfer may affect other organs such as the lung and liver. The advantages of the AAV9-based strategy in the preclinical setting outweigh cardiac-specific genetically modified murine models, which still need to be investigated.

CONCLUSIONS

Our study demonstrates that N-myristoylation of cardiomyocytes plays an essential role in pathological cardiac hypertrophy and heart failure. Modifying post-translational N-myristoylation through NMT2 could be a potential therapeutic approach to prevent cardiac remodeling.

ACKNOWLEDGMENTS The authors thank Tomiko Miura, Tomoko Ogata, and Chisato Kubo for their excellent technical assistance; Toshiyuki Suzuki for exceptional technical assistance with LC-MS/MS analysis; and Shunpei Ito and Yuto Fukuda for their experimental support.

FUNDING SUPPORT AND AUTHOR DISCLOSURES

This work was supported by the Japan Society for the Promotion of Science KAKENHI grants 22K08161 (Dr Tomita), 20K22907 (Dr Anzai), and 19K17572 (Dr Misaka). All other authors have reported that they have no relationships relevant to the contents of this paper to disclose.

ADDRESS FOR CORRESPONDENCE: Dr Tomofumi Misaka, Department of Cardiovascular Medicine, Fukushima Medical University, 1, Hikarigaoka, Fukushima 960-1295, Japan. E-mail: misaka83@fmu.ac.jp.

PERSPECTIVES

COMPETENCY IN MEDICAL KNOWLEDGE: Our study is the first to elucidate the role and regulation of N-myristoylation in the heart, characterizing the global profiling of proteins of N-myristoylation in cardiac myocytes. NMT2 played a crucial role in pathological cardiac hypertrophy and failure. An innovative click chemistry-based quantitative chemical proteomics identified distinct N-myristoylation substrates at endogenous levels. Among these targets, N-myristoylation of MARCKS exerted a regulative impact in pathological hypertrophy.

TRANSLATIONAL OUTLOOK: Modifying post-translational N-myristoylation through NMT2 could be a potential therapeutic approach to prevent cardiac remodeling. Up-regulation of NMT2 may be a novel strategy for heart failure.

REFERENCES

1. Burchfield JS, Xie M, Hill JA. Pathological ventricular remodeling: mechanisms: part 1 of 2. *Circulation*. 2013;128(4):388–400.

2. Nakamura M, Sadoshima J. Mechanisms of physiological and pathological cardiac hypertrophy. *Nat Rev Cardiol*. 2018;15(7):387–407.

3. Fert-Bober J, Murray CI, Parker SJ, Van Eyk JE. Precision profiling of the cardiovascular post-translationally modified proteome: where there is a will, there is a way. *Circ Res*. 2018;122(9):1221–1237.

4. Reimand J, Wagih O, Bader GD. Evolutionary constraint and disease associations of post-translational modification sites in human genomes. *PLoS Genet*. 2015;11(1):e1004919.

5. Lundby A, Andersen MN, Steffensen AB, et al. In vivo phosphoproteomics analysis reveals the cardiac targets of beta-adrenergic receptor signaling. *Sci Signal*. 2013;6(278):rs11.

6. Kuzmanov U, Guo H, Buchsbaum D, et al. Global phosphoproteomic profiling reveals perturbed signaling in a mouse model of dilated cardiomyopathy. *Proc Natl Acad Sci U S A*. 2016;113(44):12592–12597.

7. Resh MD. Trafficking and signaling by fatty-acylated and prenylated proteins. *Nat Chem Biol*. 2006;2(11):584–590.

8. Farazi TA, Waksman G, Gordon JI. The biology and enzymology of protein N-myristoylation. *J Biol Chem*. 2001;276(43):39501–39504.

9. Rajala RV, Datla RS, Moyana TN, et al. N-myristoyltransferase. *Mol Cell Biochem*. 2000;204(1-2):135–155.

10. Wang YC, Peterson SE, Loring JF. Protein post-translational modifications and regulation of pluripotency in human stem cells. *Cell Res*. 2014;24(2):143–160.

11. Wright MH, Clough B, Rackham MD, et al. Validation of N-myristoyltransferase as an antimalarial drug target using an integrated chemical biology approach. *Nat Chem*. 2014;6(2):112–121.

12. Frearson JA, Brand S, McElroy SP, et al. N-myristoyltransferase inhibitors as new leads to treat sleeping sickness. *Nature*. 2010;464(7289):728–732.

13. Beauchamp E, Yap MC, Iyer A, et al. Targeting N-myristoylation for therapy of B-cell lymphomas. *Nat Commun*. 2020;11(1):5348.

14. Timms RT, Zhang Z, Rhee DY, et al. A glycine-specific N-degron pathway mediates the quality control of protein N-myristoylation. *Science*. 2019;365(6448):eaaw4912.

15. Misaka T, Murakawa T, Nishida K, et al. FKBP8 protects the heart from hemodynamic stress by preventing the accumulation of misfolded proteins and endoplasmic reticulum-associated apoptosis in mice. *J Mol Cell Cardiol*. 2018;114:93–104.

16. Souders CA, Borg TK, Banerjee I, Baudino TA. Pressure overload induces early morphological changes in the heart. *Am J Pathol*. 2012;181(4):1226–1235.

17. Doroudgar S, Volkers M, Thuerauf DJ, et al. Hrd1 and ER-associated protein degradation, ERAD, are critical elements of the adaptive ER stress response in cardiac myocytes. *Circ Res*. 2015;117(6):536–546.

18. Agard NJ, Prescher JA, Bertozzi CR. A strain-promoted [3 + 2] azide-alkyne cycloaddition for covalent modification of biomolecules in living systems. *J Am Chem Soc*. 2004;126(46):15046–15047.

19. Thirumurugan P, Matosiuk D, Jozwiak K. Click chemistry for drug development and diverse chemical-biology applications. *Chem Rev*. 2013;113(7):4905–4979.

20. Keller A, Nesvizhskii AI, Kolker E, Aebersold R. Empirical statistical model to estimate the accuracy of peptide identifications made by MS/MS and database search. *Anal Chem*. 2002;74(20):5383–5392.

21. Al Shweiki MR, Monchgesang S, Majovsky P, et al. Assessment of label-free quantification in discovery proteomics and impact of technological factors and natural variability of protein abundance. *J Proteome Res*. 2017;16(4):1410–1424.

22. Kimishima Y, Misaka T, Yokokawa T, et al. Clonal hematopoiesis with JAK2V617F promotes pulmonary hypertension with ALK1 upregulation in lung neutrophils. *Nat Commun*. 2021;12(1):6177.

23. Fang H, Lai NC, Gao MH, et al. Comparison of adeno-associated virus serotypes and delivery methods for cardiac gene transfer. *Hum Gene Ther Methods*. 2012;23(4):234–241.

24. Hang HC, Wilson JP, Charron G. Bioorthogonal chemical reporters for analyzing protein lipidation and lipid trafficking. *Acc Chem Res*. 2011;44(9):699–708.

25. Seok H, Lee H, Lee S, et al. Position-specific oxidation of miR-1 encodes cardiac hypertrophy. *Nature*. 2020;584(7820):279–285.

26. Trivedi CM, Luo Y, Yin Z, et al. Hdac2 regulates the cardiac hypertrophic response by modulating Gsk3 beta activity. *Nat Med*. 2007;13(3):324–331.

27. Thinon E, Serwa RA, Broncel M, et al. Global profiling of co- and post-translationally N-myristoylated proteomes in human cells. *Nat Commun*. 2014;5:4919.

28. Kosciuk T, Price IR, Zhang X, et al. NMT1 and NMT2 are lysine myristoyltransferases regulating the ARF6 GTPase cycle. *Nat Commun*. 2020;11(1):1067.

29. Ashburner M, Ball CA, Blake JA, et al. Gene ontology: tool for the unification of biology. The Gene Ontology Consortium. *Nat Genet*. 2000;25(1):25–29.

30. Yang SH, Shrivastav A, Kosinski C, et al. N-myristoyltransferase 1 is essential in early mouse development. *J Biol Chem*. 2005;280(19):18990–18995.

31. Forrester SJ, Booz GW, Sigmund CD, et al. Angiotensin II signal transduction: an update on mechanisms of physiology and pathophysiology. *Physiol Rev*. 2018;98(3):1627–1738.

32. Kalwa H, Michel T. The MARCKS protein plays a critical role in phosphatidylinositol 4,5-bisphosphate metabolism and directed cell movement in vascular endothelial cells. *J Biol Chem*. 2011;286(3):2320–2330.

33. Kalwa H, Sartoretto JL, Sartoretto SM, Michel T. Angiotensin-II and MARCKS: a hydrogen peroxide- and RAC1-dependent signaling pathway in vascular endothelium. *J Biol Chem*. 2012;287(34):29147–29158.

34. Anderson ME, Brown JH, Bers DM. CaMKII in myocardial hypertrophy and heart failure. *J Mol Cell Cardiol*. 2011;51(4):468–473.

35. Xu JX, Si M, Zhang HR, et al. Phosphoinositide kinases play key roles in norepinephrine- and angiotensin II-induced increase in phosphatidylinositol 4,5-bisphosphate and modulation of cardiac function. *J Biol Chem*. 2014;289(10):6941–6948.

36. Backs J, Song K, Bezprozvannaya S, Chang S, Olson EN. CaM kinase II selectively signals to histone deacetylase 4 during cardiomyocyte hypertrophy. *J Clin Invest*. 2006;116(7):1853–1864.

37. Lehmann LH, Jebessa ZH, Kreusser MM, et al. A proteolytic fragment of histone deacetylase 4 protects the heart from failure by regulating the hexosamine biosynthetic pathway. *Nat Med*. 2018;24(1):62–72.

38. Parker CG, Pratt MR. Click chemistry in proteomic investigations. *Cell*. 2020;180(4):605–632.

39. Wang B, Dai T, Sun W, et al. Protein N-myristoylation: functions and mechanisms in control of innate immunity. *Cell Mol Immunol*. 2021;18(4):878–888.

40. Aderem A. The MARCKS brothers: a family of protein kinase C substrates. *Cell*. 1992;71(5):713–716.

41. Laux T, Fukami K, Thelen M, et al. GAP43, MARCKS, and CAP23 modulate PI(4,5)P(2) at plasmalemmal rafts, and regulate cell cortex actin dynamics through a common mechanism. *J Cell Biol*. 2000;149(7):1455–1472.

42. Cordeddu V, Di Schiavi E, Pennacchio LA, et al. Mutation of SHOC2 promotes aberrant protein N-myristoylation and causes Noonan-like

syndrome with loose anagen hair. *Nat Genet*. 2009;41(9):1022–1026.

43. Deng L, Gao X, Liu B, et al. NMT1 inhibition modulates breast cancer progression through stress-triggered JNK pathway. *Cell Death Dis*. 2018;9(12):1143.

44. Rowe DC, McGettrick AF, Latz E, et al. The myristoylation of TRIF-related adaptor molecule is essential for Toll-like receptor 4 signal transduction. *Proc Natl Acad Sci U S A*. 2006;103(16):6299–6304.

45. Cannata A, Ali H, Sinagra G, Giacca M. Gene therapy for the heart lessons learned and future perspectives. *Circ Res*. 2020;126(10):1394–1414.

46. Zhao Y, Zou Z, Sun D, et al. GLIPR2 is a negative regulator of autophagy and the BECN1-ATG14-containing phosphatidylinositol 3-kinase complex. *Autophagy*. 2019;17(10):2891–2904.

KEY WORDS cardiac remodeling, gene therapy, heart failure, N-myristoylation, post-translational modifications

APPENDIX For an expanded Methods section as well as supplemental tables and figures, please see the online version of this paper.